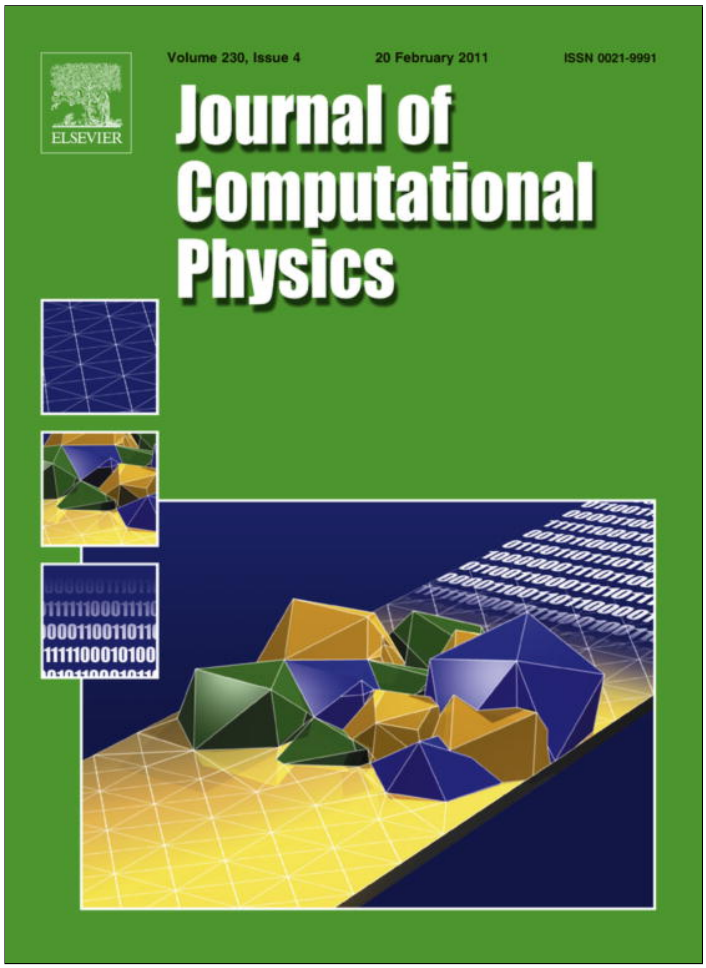

Journal of Computational Physics 230 (2011) 1370–1381

Contents lists available at ScienceDirect

Journal of Computational Physics

journal homepage: www.elsevier.com/locate/jcp

A discrete geometric approach to solving time independent Schrödinger equation

Ruben Specogna *, Francesco Trevisan

Università di Udine, Via delle Scienze 208, I-33100 Udine, Italy

ARTICLE INFO

Article history:
Received 17 May 2010
Received in revised form 28 October 2010
Accepted 3 November 2010
Available online 13 November 2010

Keywords:
Discrete geometric approach (DGA)
Cell method
Schrödinger equation

ABSTRACT

The time independent Schrödinger equation stems from quantum theory axioms as a partial differential equation. This work aims at providing a novel discrete geometric formulation of this equation in terms of integral variables associated with precise geometric elements of a pair of three-dimensional interlocked grids, one of them based on tetrahedra. We will deduce, in a purely geometric way, a computationally efficient discrete counterpart of the time independent Schrödinger equation in terms of a standard symmetric eigenvalue problem. Moreover boundary and interface conditions together with non homogeneity and anisotropy of the media involved are accounted for in a straightforward manner.

This approach yields to a sensible computational advantage with respect to the finite element method, where a generalized eigenvalue problem has to be solved instead. Such a modeling tool can be used for analyzing a number of quantum phenomena in modern nano-structured devices, where the accounting of the real 3D geometry is a crucial issue.

1. Introduction

In recent years, there has been an effort to highlight the geometric structure behind different physical theories. This idea has a solid physical and mathematical foundation, described in the works of Tonti in electromagnetism and elasticity [1,3–5], of Bossavit with the understanding of the geometric properties of the finite element method in computational electromagnetics [6,10], of Di Carlo on heat conduction [7], or of Weiland regarding the Finite Integration Technique on electromagnetic wave propagation [8,9].

The fundamental geometric structure on which the physical laws of a specific theory are based, allows us to formulate these laws in a discrete manner with respect to a pair of oriented and staggered cell complexes, one dual to the other, leading to the so-called Discrete Geometric Approach (DGA) for computational physics (some instances of this discretization process in the case of Maxwell's equations, can be found in [10–14]).

In this framework, the purpose of our paper is to show how the *modus operandi* of the DGA could be conveniently applied also to the discretization of the time independent Schrödinger equation with respect to a primal cell complex based on tetrahedra. In this way, it will be possible to provide a new computationally efficient modeling tool for a number of quantum phenomena in modern nano-structured devices, where the accounting of the real 3D geometry is a crucial issue [15–17]. In addition, the treatment of boundary and interface conditions together with non-homogeneity and anisotropy of the media involved, can also be easily accounted for.

* Corresponding author. Tel.: +39 0432 558285; fax: +39 0432 558251.
E-mail addresses: ruben.specogna@uniud.it (R. Specogna), trevisan@uniud.it (F. Trevisan).

0021-9991/$ - see front matter © 2010 Elsevier Inc. All rights reserved.
doi:10.1016/j.jcp.2010.11.007

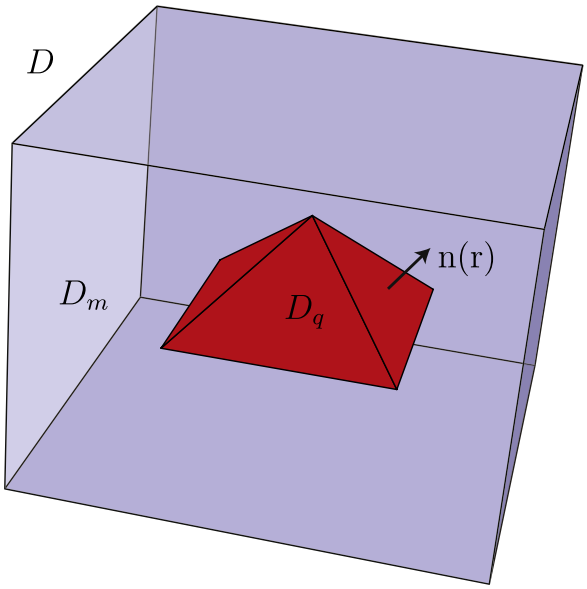

Fig. 1. Quantum dot domain D_q embedded in a matrix of different material D_m.

The paper is organized as follows. We start, in Section 2, with a reformulation of the time independent Schrödinger equation in terms of scalar, vector and tensor field quantities involved in two different categories of equations: continuous *balance* equations and *constitutive* relations.

In Section 3, after the discretization of the spatial domain into geometric elements such as nodes, edges, faces and volumes of a pair of oriented cell complexes, we will introduce integrals – such as circulations or fluxes – of the introduced field quantities with respect to nodes, edges, faces and volumes of the pair of cell complexes. In the literature, such working integral variables are often referred to as Degrees of Freedom (DoFs) or global variables. Then we will form *exact* discrete counterparts of the balance equations in terms of DoFs and we will construct *approximate* discrete counterparts of the constitutive relations transforming the DoFs associated with geometric elements of one cell complex into the corresponding (dual) DoFs associated with geometric elements of the other cell complex.

In Section 4, we will construct efficiently, in a purely geometric way, the discrete counterpart of the continuous level Schrödinger equation, by coupling the discrete counterparts of balance equations and constitutive relations. A big advantage will be apparent, since a standard symmetric eigenvalue problem will be obtained. On the contrary, Finite Elements yield a more computationally onerous generalized eigenvalue problems [17,18].

Finally, Section 5 will be dedicated to numerical results, where we will analyze, first for reference, the case of a particle within a box; then, we will move on to the analysis of a three-dimensional pyramid-shaped quantum dot heterostructure [16,20].

2. Time independent Schrödinger equation

In a three-dimensional finite spatial domain D, the time independent Schrödinger equation for a single particle [19], can be written as:

$$-\nabla \cdot \mathrm{q}(\mathrm{r})\nabla\psi(\mathrm{r}) = (\lambda - u(\mathrm{r}))\psi(\mathrm{r}), \tag{1}$$

where λ is the unknown energy level (eigenvalue) and $\psi(\mathrm{r})$ is the corresponding eigenfunction evaluated at a point r of D, individuated by the Cartesian components (x,y,z) of the position vector r[1]; $\mathrm{q}(\mathrm{r})$ is a diagonal[2] double tensor whose ijth Cartesian component, with $i, j = 1,\ldots,3$, is

$$q_{ij}(\mathrm{r}) = \frac{\hbar}{2m_i(\mathrm{r})}\delta_{ij}, \tag{2}$$

where $\hbar$ is the reduced Plank constant and $m_i(\mathrm{r})$ is the effective mass coefficient of the particle, along the ith Cartesian axis, with $i = 1,\ldots,3$, assumed here independent of λ; δ_{ij} is the Kronecker symbol. Finally, $u(\mathrm{r})$ denotes the confinement potential energy term, considered known in this paper.

Of course, boundary conditions on ∂D must be considered in addition to close the problem; in general, Dirichlet boundary conditions are imposed on a portion S_D of ∂D by fixing a prescribed value of $(\psi(\mathrm{r}))_{S_D}$ while, on the remaining part S_N of ∂D, Neumann boundary conditions $(\mathrm{n}(\mathrm{r}) \cdot \mathrm{q}(\mathrm{r})\nabla\psi(\mathrm{r}))_{S_N}$ are assigned, $\mathrm{n}(\mathrm{r})$ being the outward normal to S_N and $S_D \bigcup S_N = \partial D$.

[1] Vectors and tensors are denoted in roman type.
[2] In general, $\mathrm{q}(\mathrm{r})$ can also be non diagonal without affecting the results of this work.

In nano-scale applications, such as pyramid-shaped quantum dots [16,17], since eigenfunction $\psi(\mathrm{r})$ decays very rapidly outside the quantum dot, it is reasonable to assume homogeneous Dirichlet boundary conditions on ∂D. Moreover, the effective mass of the particle and thus the tensor $\mathrm{q}(\mathrm{r})$ are discontinuous in D. A typical example is an InAs pyramid quantum dot domain D_q embedded in a cuboid GaAs domain D_m, where $D_q \bigcup D_m = D$, Fig. 1. The discontinuity of tensor $\mathrm{q}(\mathrm{r})$ yields to the following interface conditions on surface ∂D_q

$$(\psi(\mathrm{r}))_{\partial D_q^+} = (\psi(\mathrm{r}))_{\partial D_q^-}, (\mathrm{n}(\mathrm{r}) \cdot \mathrm{q}(\mathrm{r}) \nabla \psi(\mathrm{r}))_{\partial D_q^+} = (\mathrm{n}(\mathrm{r}) \cdot \mathrm{q}(\mathrm{r}) \nabla \psi(\mathrm{r}))_{\partial D_q^-}, \tag{3}$$

where $\mathrm{n}(\mathrm{r})$ is the normal to ∂D_q, pointing outward D_q, ∂D_q^+, ∂D_q^- denote the positive and negative sides of ∂D_q respectively; the first condition expresses the continuity of $\psi(\mathrm{r})$ across ∂D_q, while the second condition is usually referred to as Ben Daniel–Duke condition [20]. In the presence of such a surface of discontinuity ∂D_q, (1) subject to (3) must be solved in $D_m \cup D_q$.

2.1. The Schrödinger equation reformulated

Now, we will reformulate in a slightly different way the left-hand side of (1), in terms of the following relations

$$-\nabla \psi(\mathrm{r}) = \mathrm{a}(\mathrm{r}), \tag{4}$$

$$\mathrm{q}(\mathrm{r})\mathrm{a}(\mathrm{r}) = \mathrm{b}(\mathrm{r}), \tag{5}$$

$$\nabla \cdot \mathrm{b}(\mathrm{r}) = \phi(\mathrm{r}), \tag{6}$$

where we introduced the vector fields $\mathrm{a}(\mathrm{r})$, $\mathrm{b}(\mathrm{r})$ and the scalar field $\phi(\mathrm{r})$ respectively; while, for the right hand side, we write

$$\xi(\mathrm{r})\psi(\mathrm{r}) = \phi(\mathrm{r}), \tag{7}$$

where

$$\xi(\mathrm{r}) = (\lambda - u(\mathrm{r})) \tag{8}$$

holds. Of course, (4)–(7) are equivalent to (1). From (4), we observe that $\psi(\mathrm{r})$ acts as a scalar potential for the *exact* field $\mathrm{a}(\mathrm{r})$ in the contractible domain D; moreover (5) and (7) play the role of constitutive relations between a pair of vector and scalar fields respectively, $\mathrm{q}(\mathrm{r})$ and $\xi(\mathrm{r})$ being the medium characteristics. This interpretation is an important modeling issue at the base of the modus operandi of DGA approach.

3. Towards a discrete counterpart of Schrödinger equation

In order to reformulate in a discrete way the Schrödinger equation casted in the form (4)–(7), we need to retrace, in the following subsections, the fundamental steps at the base of Discrete Geometric Approach [2,1].

3.1. Domain discretization

We introduce in D a primal *simplicial* cell complex $\mathcal{K} = \{\mathcal{N}, \mathcal{E}, \mathcal{F}, \mathcal{V}\}$, whose geometrical elements are nodes $n_i \in \mathcal{N}$, edges $e_j \in \mathcal{E}$, faces $f_h \in \mathcal{F}$ (triangles), and volumes $v_k \in \mathcal{V}$ (tetrahedra), all endowed with an inner orientation [2,22], Fig. 2; the cardinality of each set $\mathcal{N}, \mathcal{E}, \mathcal{F}, \mathcal{V}$ is denoted by N, E, F and V respectively.

From the primal cell complex $\mathcal{K}$, we can construct a *barycentric* dual complex $\widetilde{\mathcal{K}} = \{\widetilde{\mathcal{V}}, \widetilde{\mathcal{F}}, \widetilde{\mathcal{E}}, \widetilde{\mathcal{N}}\}$, whose geometrical elements are dual nodes $\tilde{n}_k \in \widetilde{\mathcal{N}}$, dual edges $\tilde{e}_h \in \widetilde{\mathcal{E}}$, dual faces $\tilde{f}_j \in \widetilde{\mathcal{F}}$ and dual volumes $\tilde{v}_i \in \widetilde{\mathcal{V}}$; the inner orientation of $\mathcal{K}$ induces an outer orientation of $\widetilde{\mathcal{K}}$, the cells of $\mathcal{K}$ being in a one-to-one correspondence[3] with those of $\widetilde{\mathcal{K}}$. A dual node $\tilde{n}_k$ is the barycenter of tetrahedron v_k, a dual edge $\tilde{e}_h$ is a broken segment of the line joining the barycenters of a pair of tetrahedra through the barycenter g_{f_h} of the face f_h they have in common. A dual face $\tilde{f}_j$ is the union of a number of quadrilateral faces, tailored within each tetrahedron of the cluster of tetrahedra having e_j in common; the vertices of each quadrilateral face are respectively the barycenter of a tetrahedron of the cluster, the midpoint g_{e_j} of e_j and the barycenters of the pair of primal faces having e_j in common and bounding that tetrahedron, refer to Fig. 2. Finally, a dual volume $\tilde{v}_i$ is the union of a number of hexahedral subregions tailored within each tetrahedron of the cluster of tetrahedra having n_i as common node; each subregion is delimited by a triple of primal faces having n_i in common bounding a tetrahedron of the cluster and by a triple of quadrilateral faces opposite to n_i within that tetrahedron. Without losing generality, it is convenient and computationally efficient to work element-by-element by restricting $\mathcal{K}$ to a single tetrahedron; consequently we focus on the restriction of $\widetilde{\mathcal{K}}$ to a single tetrahedron v_k, Fig. 2. The restriction in v_k of a dual edge is a segment and the restriction of a dual face is a plane quadrilateral surface; in this way the tangent and normal vectors respectively are well defined.

The interconnections of $\mathcal{K}$ are described by incidence matrices; for our purposes, we need matrix $\mathbf{G}$ of dimension $E \times N$ of incidence numbers G_{ji} between orientations of pairs (e_j, n_i), matrix $\mathbf{D}$ of dimension $V \times F$ of incidence numbers D_{kh} between the orientations of pairs (v_k, f_h) and matrix $\widetilde{\mathbf{D}}$ of dimension $N \times E$ of incidence numbers between the orientations of pairs $(\tilde{v}_i, \tilde{f}_j)$. Thanks to the duality between $\mathcal{K}, \widetilde{\mathcal{K}}$

[3] It is often referred to as *duality*.

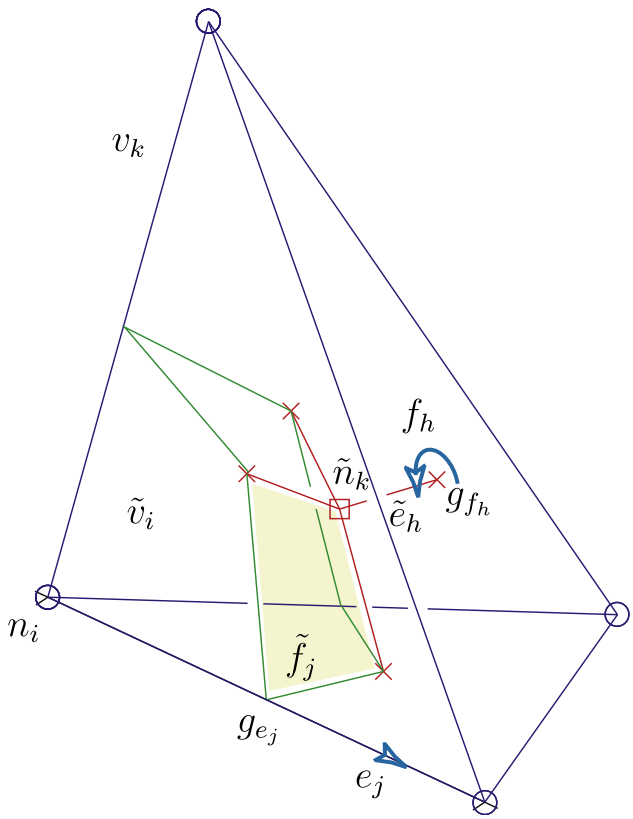

Fig. 2. Oriented geometric elements of the primal complex $\mathcal{K}$ and of the dual complex $\widetilde{\mathcal{K}}$ restricted, for clarity, to a single tetrahedron v_k.

$$\widetilde{\mathbf{D}} = -\mathbf{G}^T \tag{9}$$

holds.[4]

3.2. Integral variables and their association to the elements of $\mathcal{K}, \widetilde{\mathcal{K}}$

We introduce array $\mathbf{\Psi}$ of dimension N, whose ith entry

$$\Psi_i = \psi(\mathrm{r}_{n_i}), \quad i = 1, \ldots, N \tag{10}$$

is the value $\psi(\mathrm{r}_{n_i})$ assumes in the position r_{n_i} of the node n_i; clearly, Ψ_i is associated with primal nodes.

Circulation A_j of vector $\mathrm{a}(\mathrm{r})$ along a primal edge e_j is defined by

$$A_j = \int_{e_j} \mathrm{a}(\mathrm{r}) \cdot d\mathrm{l} \tag{11}$$

with $j = 1, \ldots, E$, and it is associated with primal edges; the array $\mathbf{A}$ they form has dimension E. Similarly, but at a different geometric level, flux B_j of vector $\mathrm{b}(\mathrm{r})$ across a dual face $\tilde{f}_j$ is defined by

$$B_j = \int_{\tilde{f}_j} \mathrm{b}(\mathrm{r}) \cdot d\mathrm{s} \tag{12}$$

with $j = 1, \ldots, E$, associated with dual faces and the array $\mathbf{B}$ they form has dimension E.

Finally, we introduce the integral quantity

$$\Phi_i = \int_{\tilde{v}_i} \phi(\mathrm{r}) dv \tag{13}$$

associated with dual volume $\tilde{v}_i$, with $i = 1, \ldots, N$, and we denote with $\mathbf{\Phi}$ the corresponding array they form, of dimension N.

The arrays $\mathbf{\Psi}$, $\mathbf{A}$, $\mathbf{B}$ and $\mathbf{\Phi}$ of integral variables are often referred to as Degrees of Freedom (DoF) or *global* variables arrays and we observe that the arrays $\mathbf{A}$, $\mathbf{B}$ are one dual of the other being associated with dual geometric elements of the sets $\mathcal{E}$, $\widetilde{\mathcal{F}}$ respectively; similarly for the pair $\mathbf{\Psi}$, $\mathbf{\Phi}$, being associated with the dual geometric elements of the sets $\mathcal{N}, \widetilde{\mathcal{V}}$ respectively.

[4] The minus sign comes from the assumption that n_i is oriented as a sink, whereas the boundary of $\tilde{v}_i$ is oriented by the outer normal.

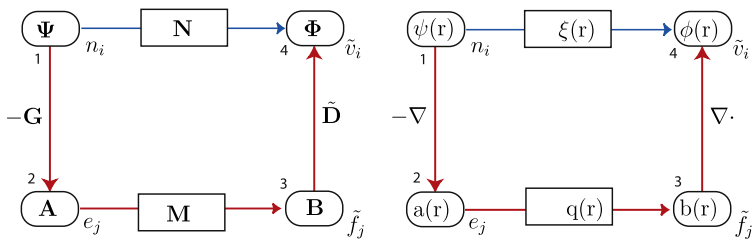

Fig. 3. Tonti's diagram for discrete (left side) and continuous (right side) Schrödinger equations.

3.3. Balance equations

Now, according to algebraic topology [2,1], we can straightforwardly construct *exact*[5] discrete counterparts of (4) and (6) respectively, in terms of the introduced DoF arrays with respect to the topology of the pair of cell complexes $\mathcal{K}, \widetilde{\mathcal{K}}$ and we obtain

$$-\mathbf{G}\boldsymbol{\Psi} = \mathbf{A}, \tag{14}$$

$$\widetilde{\mathbf{D}}\mathbf{B} = -\mathbf{G}^T\mathbf{B} = \boldsymbol{\Phi}, \tag{15}$$

where in (15) we used (9); these relations are independent of the media and metric of the pair of cell complexes in D.

3.4. Constitutive relations

A crucial point of the discretisation process is the computation of discrete counterparts of the constitutive relations (5) and (7) at continuous level. Such discrete counterparts can be represented as linear operators (matrices in our case) mapping DoF arrays in a duality relation. Therefore the discrete counterparts for (5) and (7) can be written as:

$$\mathbf{M}\mathbf{A} = \mathbf{B}, \tag{16}$$

$$\mathbf{N}\boldsymbol{\Psi} = \boldsymbol{\Phi}, \tag{17}$$

where $\mathbf{M}$ and $\mathbf{N}$ are square matrices of dimension E and N respectively, depending on the metric and media properties of the pair of cell complexes. It is important to note that $\mathbf{M}$ and $\mathbf{N}$ are *approximated* discrete counterparts of q(r) and ξ(r) respectively. There are several approaches, borrowed from different physical theories that can be applied to construct matrix $\mathbf{M}$, like those described in [21,7,12–14,11]; on the contrary, in this paper, we will follow in sub Section 4.1 a different methodology, more efficient from the computational viewpoint. On the other hand, sub Section 4.2 will be dedicated to the computation of the matrix $\mathbf{N}$.

3.5. A discrete Schrödinger equation

In order to underline the geometric structure behind Schrödinger equation, both in the discrete setting and in the continuous setting, and to deduce the algebraic system of equations discretizing Schrödinger equation, we will introduce the so called *Tonti's diagram* (for a comprehensive description for other physical theories see [1,3]), specifically tailored for our problem, Fig. 3.

For time independent problems, the diagram (on the left part of Fig. 3) consists of two vertical pillars, where each DoF array, typed inside an oval, is associated with the corresponding geometric entity of the primal cell complex $\mathcal{K}$ (n_i, e_j from top to bottom respectively) and of the dual complex $\widetilde{\mathcal{K}}$ ($\tilde{f}_j$, $\tilde{v}_i$ from bottom to top respectively). Along a vertical pillar, we move from the variables associated with a geometric entity to the variable associated with the successive geometric entity, of the primal or of the dual complex, using the incidence matrices ($\mathbf{G}$, or $\widetilde{\mathbf{D}}$ in the specific case). The duality is made evident in the diagram, where geometric entities and associated DoF arrays, on the left and right parts of the diagram, correspond each other along horizontal lines. The discrete counterparts of the constitutive relations are represented as horizontal links from left to right. The association of DoF arrays to the geometric elements of the pair of complexes, induces a similar association between the corresponding scalar/vector field quantities as shown by the Tonti's diagram on the right side of Fig. 3; moreover, the relation between discrete level and continuous level constitutive relations is apparent from the diagram together with the discrete, metric free, counterparts $-\mathbf{G}$, $\widetilde{\mathbf{D}}$ of the continuous level operators $-\nabla$, $\nabla\cdot$ respectively. Finally, we may deduce a discrete counterpart of Schrödinger equation working on the discrete diagram (left part of Fig. 3). By following the path 1–2–3–4 we obtain

$$\mathbf{G}^T\mathbf{M}\mathbf{G}\boldsymbol{\Psi} = \boldsymbol{\Phi} \tag{18}$$

which is a discrete counterpart of the left-hand side of (1), while the path 1–4 yields

$$\mathbf{N}\boldsymbol{\Psi} = \boldsymbol{\Phi}, \tag{19}$$

[5] This means that array $\boldsymbol{\Psi}$ is mapped exactly onto array $\boldsymbol{\Phi}$ provided that the fields are locally uniform in tetrahedron v_k.

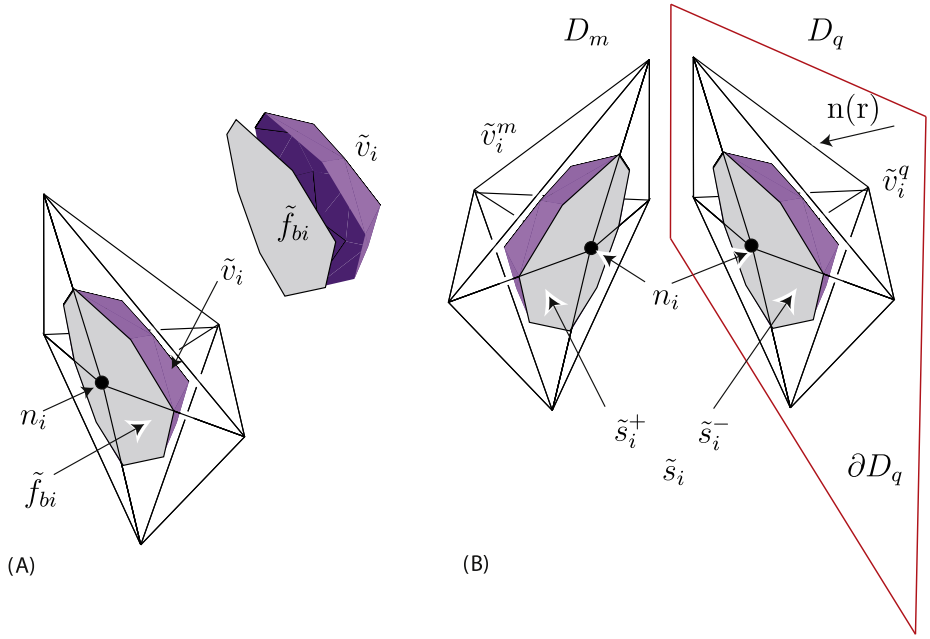

Fig. 4. (A): Additional dual boundary face $\tilde{f}_{bi}$ in a one-to-one correspondence with node n_i on $S_N \subset \partial D$ and the corresponding dual volume $\tilde{v}_i$ are shown. (B): A dual volume $\tilde{v}_i$ in a one-to-one correspondence with node n_i on ∂D_q is exploded for clarity, together with the pair of sides $\tilde{s}_i^+, \tilde{s}_i^-$ of the dual face $\tilde{s}_i$ in a one-to-one correspondence with n_i.

which is a discrete counterpart of the right hand side of (1). Thus, from (18) and (19) a discrete counterpart of (1) becomes

$$\mathbf{G}^T\mathbf{M}\mathbf{G}\boldsymbol{\Psi} = \mathbf{N}\boldsymbol{\Psi}. \tag{20}$$

3.6. Discrete boundary and interface conditions

Discrete Dirichlet boundary conditions on the portion of boundary S_D are imposed by assigning Ψ_i values on the primal nodes on S_D. Homogeneous Dirichlet boundary conditions are simply enforced by skipping the values of Ψ_i relative to primal nodes on S_D. Such Ψ_i are not an unknown of the problem, hence the corresponding equations in (20) are not written.

Discrete Neumann boundary conditions on S_N are simply accounted for by assigning the values of B_i associated with additional boundary dual faces $\tilde{f}_{bi}$ on S_N in a one-to-one correspondence with the primal nodes on S_N, Fig. 4(A); discrete homogeneous Neumann boundary conditions on S_N are naturally accounted for in (20) since $B_i = 0$ on $\tilde{f}_{bi}$ is assumed.

Discrete interface conditions (3) on discontinuity surfaces in D are automatically accounted for due to the continuity of the circulations A_j along primal edges e_j on such discontinuity surfaces; this yields in turn the continuity of the potential $\psi(\mathrm{r})$ on primal nodes belonging to such surfaces. Also the Ben Daniel–Duke interface condition is automatically satisfied in the discrete setting. To show this, let us consider a primal node n_i on a discontinuity surface ∂D_q, refer to Fig. 4(B), and the corresponding dual volume $\tilde{v}_i$ divided by ∂D_q in two parts $\tilde{v}_i^m, \tilde{v}_i^q$ in D_m, D_q subregions respectively; dual face $\tilde{s}_i$ in a one-to-one correspondence with n_i lies on ∂D_q and $\tilde{s}_i^+, \tilde{s}_i^-$ denote its two sides. By particularizing (15) for $\tilde{v}_i^m, \tilde{v}_i^q$ we obtain respectively

$$\sum_{k\in\mathcal{E}_i^m} \pm B_k^m - B_{\tilde{s}_i} = \Phi_i^m, \quad \sum_{k\in\mathcal{E}_i^p} \pm B_k^p + B_{\tilde{s}_i} = \Phi_i^q, \tag{21}$$

where $\pm B_k^m, \pm B_k^p$ are fluxes, weighted by incidence numbers, associated with dual faces in D_m, D_q indexed in the sets $\mathcal{E}_i^m, \mathcal{E}_i^p$ respectively; Φ_i^m, Φ_i^q are the values variable Φ_i assumes in D_m, D_q respectively.

Flux $B_{\tilde{s}_i}$ is associated with $\tilde{s}_i$ and, of course, it is continuous between the $\tilde{s}_i^+, \tilde{s}_i^-$ sides of $\tilde{s}_i$ as the Ben Daniel–Duke condition prescribes at a discrete level. When assembling the balance equation for the entire dual volume $\tilde{v}_i = \tilde{v}_i^m \bigcup \tilde{v}_i^q$, (22) yields

$$\sum_{k\in\mathcal{E}_i} \pm B_k = \Phi_i, \tag{22}$$

where $\Phi_i = \Phi_i^m + \Phi_i^q$ holds in $\tilde{v}_i, \mathcal{E}_i$ being the set of primal edges drawn from n_i.

4. Efficient computation of $\mathbf{G}^T\mathbf{M}\mathbf{G}$ and $\mathbf{N}$ matrices

Here, we will compute in a purely geometric way both the so called stiffness matrix $\mathbf{G}^T\mathbf{M}\mathbf{G}$ on the left-hand side of (20) and the matrix $\mathbf{N}$ on the right-hand side. The geometric approach we pursue leads to an efficient computation of the stiffness matrix in terms of the geometric entities of the primal cell complex and to a diagonal matrix $\mathbf{N}$; therefore (20) will yield to a

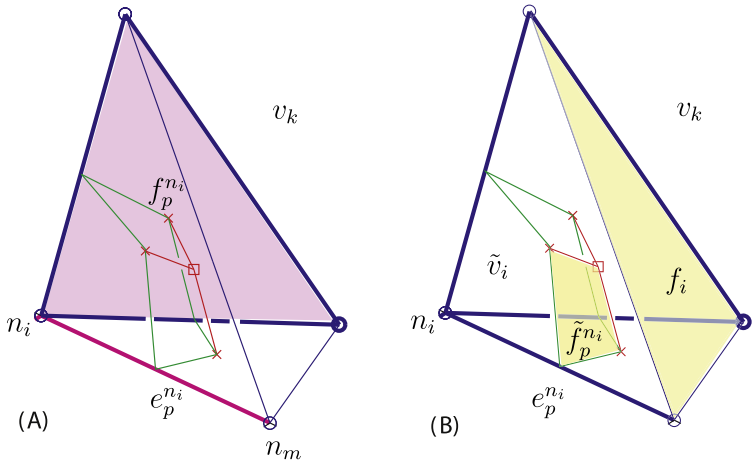

Fig. 5. Primal and dual complexes limited to a single tetrahedron v_k.

classical eigenvalue problem; on the contrary, a Finite Elements discretization leads to a generalized eigenvalue problem, which is more onerous to solve.

In the following, without loosing generality, we will focus on a single tetrahedron v_k of the primal complex, Fig. 5. With respect to v_k we will compute local $(\mathbf{G}^T\mathbf{M}\mathbf{G})^k$ and $(\mathbf{N})^k$ matrices, with $k = 1,\ldots,V$; the corresponding global matrices $\mathbf{G}^T\mathbf{M}\mathbf{G}$ and $\mathbf{N}$ are easily deduced, by adding the local contributions from each tetrahedron of the complex according to a standard assembling process.

At the base of the computation there is the assumption of local *uniformity* of scalar, vector and tensor field quantities within each tetrahedron v_k with $k = 1,\ldots,V$, since, within a small enough region, any regular field quantity can be approximated by a *uniform* field.

4.1. Computation of local stiffness matrix

We denote with n_i, $i = 1,\ldots,4$, the four nodes of tetrahedron v_k and introduce the pair $(e_p^{n_i}, f_p^{n_i})$ formed by a primal edge $e_p^{n_i}$ and a not coplanar primal face $f_p^{n_i}$ of v_k, having node n_i in common, with $p = 1,\ldots,3$, $i = 1,\ldots,4$, Fig. 5(A); correspondingly, $\mathrm{e}_p^{n_i}, \mathrm{f}_p^{n_i}$ denote edge vector[6] and face vector[7] associated with $e_p^{n_i}, f_p^{n_i}$ respectively. Then the following, purely geometric, tensor identity[8]

$$\sum_{p=1}^{3} D_{kp}\mathrm{f}_p^{n_i} \otimes G_{pi}\mathrm{e}_p^{n_i} = 3\ \mathrm{I}|v_k|, \tag{23}$$

holds, where symbol $\otimes$ denotes the tensor product, I is the identity tensor, $|v_k|$ is the volume of v_k, G_{pi} is the incidence number (± 1) between the inner orientations of $e_p^{n_i}$ and n_i, while D_{kp} is the incidence number (± 1) between the inner orientations of v_k and $f_p^{n_i}$. By right multiplying (23) by vector a(r) locally *uniform* in v_k, we obtain

$$\mathrm{a} = \frac{1}{3|v_k|}\sum_{p=1}^{3} D_{kp}G_{pi}A_p^{n_i}\ \mathrm{f}_p^{n_i}, \tag{24}$$

where we used (11). Now, denoting with (n_i, n_m) the boundary nodes of the edge e_p, with $i, m = 1,\ldots,4$ and $m \neq i$, then

$$G_{pi} = -G_{pm} \tag{25}$$

holds; using (14) for the case of tetrahedron v_k and (25), we obtain

$$A_p^{n_i} = G_{pi}(\Psi_{n_i} - \Psi_{n_m}). \tag{26}$$

Substituting (26) for $A_p^{n_i}$ in (24), we write

$$\mathrm{a} = \frac{1}{3|v_k|}\sum_{p=1}^{3} D_{kp}\ \mathrm{f}_p^{n_i}(\Psi_{n_i} - \Psi_{n_m}). \tag{27}$$

Since

[6] It is the vector having as amplitude the length of the edge, directed and oriented as the edge.
[7] It is the vector having as amplitude the area of the face, normal to the face and oriented in a congruent way as the orientation of the face.
[8] The identity stems from the geometric interpretation of a triple of vectors forming a base in $\mathbb{R}^3$ and the triple of vectors forming its *reciprocal* base [23].

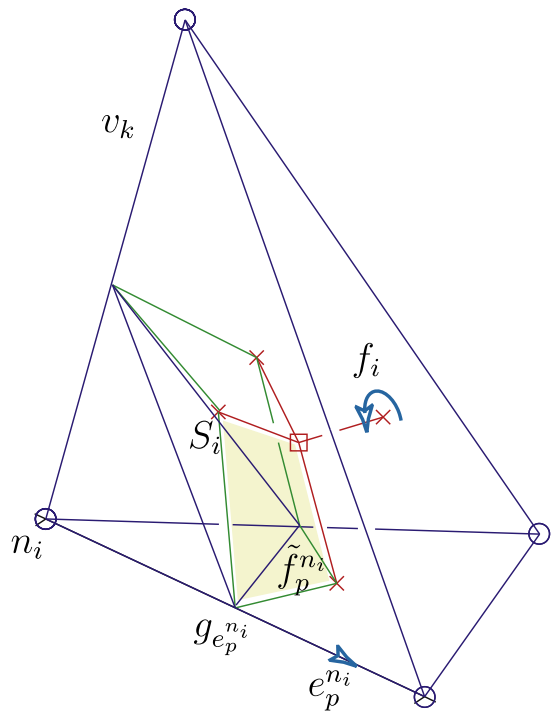

Fig. 6. Triangle S_i having as vertices the midpoints $g_{e_p^{n_i}}$ of the triple of edges $e_p^{n_i}$ drawn from the common node n_i; the area of triangle S_i is 1/3 of the area of f_i.

$$\sum_{h=1}^{4} D_{kh} \mathrm{f}_h = 0 \tag{28}$$

holds for a tetrahedron, where f_h is the area vector of the face f_h bounding v_k, then (27) becomes

$$\mathrm{a} = \frac{1}{3|v_k|} \sum_{j=1}^{4} D_{kj} \mathrm{f}_j \Psi_{n_j}, \tag{29}$$

where f_j denotes the area vector of face f_j opposite to node n_j.

Next, assuming a material tensor q(r) locally uniform in v_k, (5) implies the local uniformity of b (r) in v_k and (12) yields

$$B_p^{n_i} = \tilde{\mathrm{f}}_p^{n_i} \cdot \mathrm{qa}, \quad i = 1, \ldots, 4, \tag{30}$$

where $\tilde{\mathrm{f}}_p^{n_i}$ is the area vector associated with dual face $\tilde{f}_p^{n_i}$ in a one-to-one correspondence with $e_p^{n_i}$, with $p = 1, \ldots, 3$, Fig. 5(B). By particularizing (15) for v_k and node n_i, we write[9]

$$-\sum_{p=1}^{3} G_{ip} B_p^{n_i} = \Phi_i^k, \tag{31}$$

where we used (9), and substituting (30) for $B_p^{n_i}$ (31) yields

$$-\sum_{p=1}^{3} G_{ip} \tilde{\mathrm{f}}_p^{n_i} \cdot \mathrm{q\ a} = \Phi_i^k. \tag{32}$$

Now, from elementary geometry, we observe that the amplitude of area vector $\mathrm{S}_i = -\sum_{p=1}^{3} G_{ip} \tilde{\mathrm{f}}_p^{n_i}$ coincides with the area of the triangle S_i having as vertices the midpoints $g_{e_p^{n_i}}$ of the triple of edges $e_p^{n_i}$ drawn from the common node n_i and that from (9) $-G_{ip} = \widetilde{D}_{pi}$ holds, with $p = 1, \ldots, 3$, Fig. 6; in turns the area of S_i is $\frac{1}{3}$ of the area of f_i and in terms of area vectors

$$-\sum_{p=1}^{3} G_{ip} \tilde{\mathrm{f}}_p^{n_i} = \frac{1}{3} D_{ki}\ \mathrm{f}_i \tag{33}$$

holds, D_{ki} being the incidence number between v_k and f_i, with $i = 1, \ldots, 4$.

Finally, by substituting (33) and (29) for a in (32), we obtain

[9] The contributions due to the fluxes across the portions of the primal faces $f_p^{n_i} \cap \tilde{v}_i$, with $p = 1, \ldots, 3$, are omitted, since they cancel out in the assembly process of the entire dual volume.

$$\frac{1}{9|v_k|}\sum_{j=1}^{4} D_{ki}\mathrm{f}_i \cdot \mathrm{q} D_{kj}\ \mathrm{f}_j \Psi_{n_j} = \Phi_i^k, \tag{34}$$

It is important to note, that (34) is an *exact* discrete counterpart of (4)–(6) or, equivalently, of the left-hand side of (1) in v_k, provided that a(r), b(r), q(r) are locally *uniform* in v_k.

Therefore, from (34), the entry $(\mathbf{G}^T\mathbf{M}\mathbf{G})_{ij}^k$ of a local symmetric stiffness matrix for tetrahedron v_k, expressed efficiently in a pure geometric way, is given by:

$$(\mathbf{G}^T\mathbf{M}\mathbf{G})_{ij}^k = \frac{1}{9|v_k|} D_{ki}\mathrm{f}_i \cdot\ \mathrm{q} D_{kj}\mathrm{f}_j, \quad i,j = 1,\ldots,4. \tag{35}$$

4.2. Computation of local **N** matrix

We introduce in a tetrahedron v_k a scalar function $w_i(\ \mathrm{r})$, attached to a primal node n_i, defined as

$$w_i(\mathrm{r}) = \begin{cases} 1 & \text{if } \mathrm{r} \in \tilde{v}_i \\ 0 & \text{elsewhere} \end{cases}, \tag{36}$$

$\tilde{v}_i$ being the dual volume corresponding to n_i, Fig. 5. These base functions are able to represent exactly a locally uniform scalar field $\psi(\mathrm{r})$ in v_k as

$$\psi(\mathrm{r}) = \sum_{j=1}^{4} w_j(\mathrm{r})\Psi_j, \tag{37}$$

where we used (10). Next, using constitutive Eqs. (7), (13) yields

$$\Phi_i = \int_{\tilde{v}_i} \xi(\mathrm{r})\psi(\mathrm{r})dv. \tag{38}$$

By substituting (8) for $\xi(\mathrm{r})$ and assuming a locally uniform $\psi(\mathrm{r})$ in $\tilde{v}_i$, for $i = 1,\ldots,4$, (38) becomes

$$\Phi_i = \lambda\psi(\mathrm{r})|\tilde{v}_i| - \int_{\tilde{v}_i} u(\ \mathrm{r})\psi(\mathrm{r})dv. \tag{39}$$

From the identity $\int_{v_k} w_i(\mathrm{r})dv = |\tilde{v}_i|$ applied to the first addendum of (39), we may write

$$\Phi_i = \lambda\int_{v_k} w_i(\mathrm{r})\psi(\mathrm{r})dv - \int_{\tilde{v}_i} u(\mathrm{r})\psi(\mathrm{r})dv \tag{40}$$

and by substituting in (40), (37) for $\psi(\mathrm{r})$, we obtain

$$\Phi_i = \sum_{j=1}^{4}\left[\lambda\int_{v_k} w_i(\mathrm{r})w_j(\ \mathrm{r})dv - \int_{\tilde{v}_i} w_j(\mathrm{r})u(\mathrm{r})dv\right]\Psi_j = \tag{41}$$

$$\sum_{j=1}^{4}\lambda\delta_{ij}\frac{|v_k|}{4}\Psi_j - \sum_{j=1}^{4}\delta_{ij}\int_{\tilde{v}_i} u(\mathrm{r})dv\Psi_j, \tag{42}$$

where we used the geometric identity $|v_k| = 4|\tilde{v}_i|$, for $i = 1,\ldots,4$.

Again, it is important to note, that (42) is an *exact*[10] discrete counterpart of (7) or, equivalently, of the right hand side of (1) in v_k, provided that $\psi(\mathrm{r})$ is locally *uniform* in v_k.

Therefore, from (42), the entry $(\mathbf{N})_{ij}^k$ of a local diagonal matrix $\mathbf{N}^k$ for tetrahedron v_k, expressed efficiently in a purely geometric way, is given by:

$$(\mathbf{N})_{ij}^k = \delta_{ij}\frac{|v_k|}{4}\lambda - \delta_{ij}\int_{\tilde{v}_i} u(\mathrm{r})dv. \tag{43}$$

Such a relation, suggests to express the local matrix $\mathbf{N}^k$ as the sum of a pair of diagonal matrices

$$(\mathbf{N})^k = \lambda(\mathbf{N})'^k - (\mathbf{N}_u)^k, \tag{44}$$

whose entries are $\delta_{ij}\frac{|v_k|}{4}, \delta_{ij}\int_{\tilde{v}_i} u(\mathrm{r})dv$ respectively.

In this paper we will assume an element wise uniform potential energy $u(\mathrm{r})$ distribution in each v_k; therefore for the entries of $(\mathbf{N}_u)^k$ we simply write $\delta_{ij}\frac{|v_k|}{4}u^k$, where u^k is the uniform value $u(\mathrm{r})$ assumes in v_k.

[10] This means that array $\mathbf{\Psi}$ is mapped exactly onto array $\mathbf{\Phi}$ provided that the fields are locally uniform in tetrahedron v_k.

4.3. The discrete eigenvalue problem

For tetrahedron v_k, from (35) and (44) a generalized eigenvalue problem is obtained as

$$((\mathbf{G}^T\mathbf{M}\mathbf{G})^k + (\mathbf{N}_u)^k)\mathbf{\Psi}^k = \lambda(\mathbf{N})'^k\mathbf{\Psi}^k, \tag{45}$$

$\mathbf{\Psi}^k$ being a local array of the Ψ_i^k values, with $i = 1,\ldots,4$, in the nodes of v_k; by assembling the contributions from (45) primal volume by primal volume, for $k = 1,\ldots,V$, we obtain the final global generalized eigenvalue problem

$$(\mathbf{G}^T\mathbf{M}\mathbf{G} + \mathbf{N}_u)\mathbf{\Psi} = \lambda\mathbf{N}'\mathbf{\Psi}, \tag{46}$$

that can be easily transformed into a standard one, since $\mathbf{N}'$ is diagonal and positive-definite; we may write

$$(\mathbf{N}')^{-1/2}(\mathbf{G}^T\mathbf{M}\mathbf{G} + \mathbf{N}_u)(\mathbf{N}')^{-1/2}\mathbf{\Psi}' = \lambda\mathbf{\Psi}', \tag{47}$$

where we set $\mathbf{\Psi}' = (\mathbf{N}')^{1/2}\mathbf{\Psi}$. We observe that there is no need to compute the matrix products in (47); it is enough to multiply each non-zero ij-entry of the sparse matrix $(\mathbf{G}^T\mathbf{M}\mathbf{G} + \mathbf{N}_u)$ by $(\mathbf{N}')_i^{-1/2}(\mathbf{N}')_j^{-1/2}$ with $i, j = 1,\ldots,N$, where $(\mathbf{N}')_i^{-1/2}$ denotes the ith diagonal element of $(\mathbf{N}')^{-1/2}$.

5. Numerical results

The formulation described in this paper has been integrated into the GAME (Geometric Approach to Maxwell's Equations) code [24] developed by the Authors. The software has been implemented in Fortran 90 and the Intel Fortran 90 Compiler has been used to produce the executable. The TRLan [25] software library has been employed to solve the discrete eigenvalue problem (47). The hardware used for the computations consists of an Intel Core 2 Duo T7700 2.4 GHz laptop with 4 GB of RAM.

To validate the results produced by the described formulation, a particle in a box benchmark – which admits an analytical solution [19] – has been first analyzed. This benchmark consists of a cube of edge $d = 10$ nm in which the energy $u = 0$ eV is assumed. In our test, the material property q is described by the homogeneous, anisotropic diagonal tensor $q = \mathrm{diag}(0.04159, 0.20053, 0.20053)$.

As a second benchmark, the pyramidal quantum dot presented in [16] has been considered. It consists of a pyramid InAs quantum dot (pyramid base $d = 12.4$ nm, pyramid height $h = 6.2$ nm, $q_{InAs} = 1.5877$) placed in a GaAs matrix ($d_{box} = 24.8$ nm, $h_{box} = 18.6$ nm, $q_{GaAs} = 0.5687$), see Fig. 7. The energy of $u_{InAs} = 0$ eV is considered in the quantum dot subregion D_q, while $u_{GaAs} = 0.77$ eV is fixed in the surrounding matrix subregion D_m. On each boundary node n_i on the boundary of the cubical domain D, homogeneous Dirichlet boundary conditions $\Psi_i = 0$ have been imposed. The obtained results from the two benchmarks in term of the three smaller eigenvalues are shown in Tables 1 and 2 respectively. In these Tables, the pre-processing time t_P accounts for the time spent for the assembling of the sparse matrices in (47), while t_S is the time spent by the eigenvalue solver (TRLan).

In Fig. 8, the convergence of the error on the smallest eigenvalue is shown for the particle in a box benchmark with the mesh refinement. The mean length l_{med} of the mesh edges is considered to quantify the grain of the mesh during the refinement process. The error ϵ_{λ_1} between the computed λ_1 and analytical reference λ_{ref} values of the first eigenvalue, has been evaluated as $\epsilon_{\lambda_1} = (\lambda_1 - \lambda_{ref})/\lambda_{ref}$. The $O(h^2)$ curve represents the second order rate of convergence.

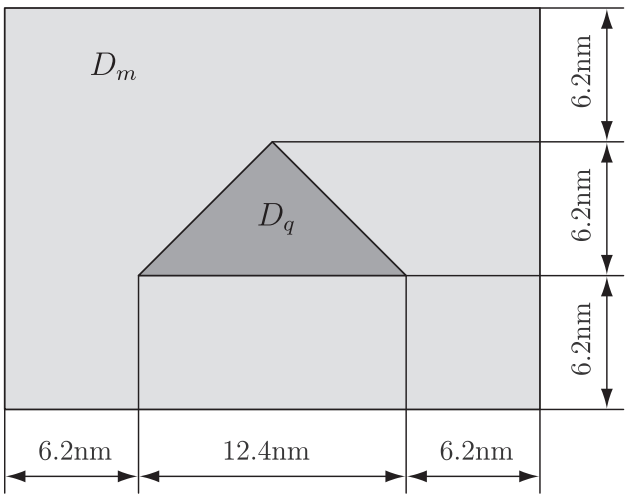

Fig. 7. Median cross-section of the three-dimensional geometry of the considered pyramidal quantum dot subregion D_q in the surrounding matrix D_m.

Table 1
Convergence with mesh refinement of the three smaller eigenvalues for the particle in a box benchmark.

V	N	t_P [s]	t_S [s]	λ_1 (% error)	λ_2 (% error)	λ_3 (% error)
928	254	<1	<1	0.04164 (−4.68)	0.05342 (−4.61)	0.06999 (−8.53)
9073	1884	<1	<1	0.04320 (−1.10)	0.05531 (−1.23)	0.07556 (−1.27)
83,493	15,578	<1	2.1	0.04355 (−0.31)	0.05581 (−0.34)	0.07624 (−0.38)
104,325	20,176	<1	3.3	0.04357 (−0.27)	0.05580 (−0.34)	0.07623 (−0.38)
393,453	71,642	<1	24.1	0.04364 (−0.12)	0.05592 (−0.13)	0.07646 (−0.09)
1,199,652	214,965	3.4	140.2	0.04366 (−0.06)	0.05596 (−0.07)	0.07648 (−0.07)
Analytic	–	–	–	0.04368 (-)	0.05600 (-)	0.07652 (-)

Table 2
Convergence with mesh refinement of the three smaller eigenvalues for the pyramidal quantum dot benchmark.

V	N	t_P [s]	t_S [s]	λ_1	λ_2	λ_3
70,439	12,434	<1	<1	0.4014	0.6428	0.6431
150,000	26076	<1	3.9	0.3956	0.6405	0.6405
293,482	50,670	<1	10.6	0.3939	0.6396	0.6396
811,552	139,462	2.1	71.2	0.3923	0.6388	0.6388
1,301,216	222,515	3.8	228.1	0.3920	0.6386	0.6386
Ref. [16]	–	–	–	0.3911	0.6380	0.6380

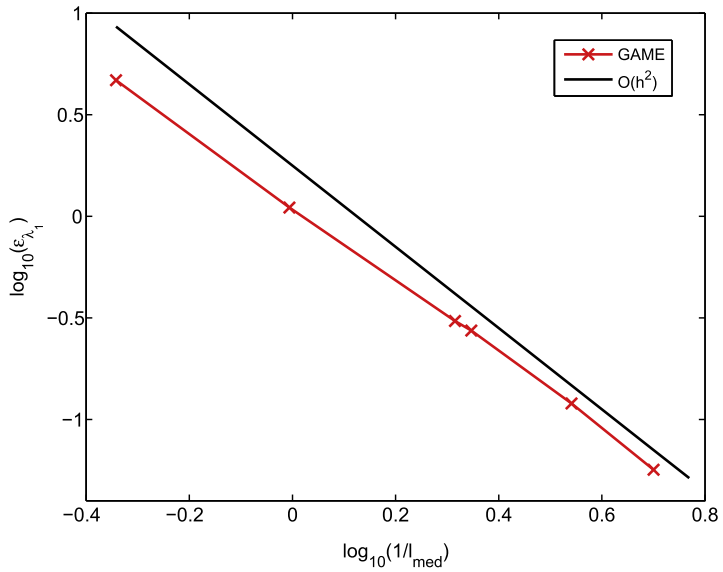

Fig. 8. Convergence of the error on the smallest eigenvalue (λ_1) with mesh refinement for the particle in a box benchmark.

6. Conclusions

We proposed a novel interpretation of the time independent Schrödinger equation which puts the spot of the light on the geometrical structure behind the variables and the balance laws of a physical theory, instead of the usual differential formulation. In this way, we introduced scalar and vector field quantities together with their edge, face and volume integrals univocally associated with the corresponding geometric elements of a pair of interlocked grids, the primal consisting of tetrahedra. This aspect is emphasized by constructing the Tonti's diagram, both at continuous and at discrete levels.

We also demonstrated how to geometrically and efficiently build a discrete counterpart of the Schrödinger equation together with boundary and interface conditions at discrete level; such a discrete counterpart is *exact* for element wise uniform fields in each tetrahedron. The proposed approach leads to a standard symmetric eigenvalue problem, the matrix on the right hand side being diagonal. Computationally, this is a big advantage compared with Finite Elements, where a symmetric generalized eigenvalue problem is obtained instead. Dealing with a generalized eigenvalue problem requires to store also the FEM "mass matrix" on the right-hand side, which has the same sparsity pattern (and hence the same memory occupation) as the "stiffness matrix" on the left-hand side. Hence, the memory requirements of DGA are exactly half of those of FEM and the mass matrix needs not to be assembled. On the contrary, Finite Elements need to convert the generalized eigenvalue problem to a standard eigenvalue problem by means of the Cholesky factorization which, notoriously, is heavy to be computed and it could be numerically unstable.

Finally, the approach proposed in this paper allows complex structures to be modeled, such as pyramidal quantum dots, in a reduced computational time, while keeping a second order convergence rate; it can also be profitably coupled with an electrostatics model, to solving a coupled *Schrödinger-Poisson* problem.

Acknowledgments

The Authors are grateful to prof. E. Tonti of the University of Trieste (Trieste, Italy) for the helpful discussions concerning the diagrams and to prof. W. Wang of the National Taiwan University for the geometrical and material data concerning the quantum dot model.

References

[1] E. Tonti, On the formal structure of physical theories, Quaderni dei Gruppi di Ricerca Matematica del CNR (1975).
[2] E. Tonti, Algebraic topology and computational electromagnetism, in: 4th International Workshop on Electric and Magnetic Fields, Marseille (Fr) 15-15 May, pp. 284–294, 1998.
[3] E. Tonti, On the geometrical structure of elecromagnetism, in: Gravitation, Electromagnetism and Geometrical Structures for the 80th birthday of A. Lichnerowicz, G. Ferrarese, Ed. Bologna, Italy: Pitagora Editrice, pp. 281–308, 1995.
[4] E. Tonti, A direct discrete formulation of field laws: the Cell Method, CMES: Comput. Model. Eng. Sci. 2 (2001) 237–258.
[5] E. Tonti, F. Zarantoello, Algebraic formulation of elastostatics: the cell method, CMES: Comput. Model. Eng. Sci. 39 (2009) 201–236.
[6] A. Bossavit, How weak is the "weak solution" in finite element methods?, IEEE Trans Mag. 34 (5) (1998) 2429–2432.
[7] A. Di Carlo, A. Tiero, The geometry of linear heat conduction, in: W. Schneider, H. Troger, F. Ziegler, (Eds.), Trends in Applications of Mathematics to Mechanics, Longman (Harlow), pp. 281–287, 1991.
[8] T. Weiland, Time domain electromagnetic field computation with finite difference methods, Int. J. Numer. Model. 9 (1996) 295–319.
[9] M. Clemens, T. Weiland, Discrete electromagnetism with the finite integration technique, in: F.L. Teixeira (Ed.), PIER32, EMW Publishing, Cambridge, Massachusetts, USA, 2001, pp. 65–87.
[10] A. Bossavit, L. Kettunen, Yee-like schemes on a tetrahedral mesh, Int. J. Numer. Model. 12 (1999) 129–142.
[11] F. Trevisan, L. Kettunen, Geometric interpretation of finite dimensional eddy current formulations, Int. J. Numer. Methods Eng. 67 (13) (2006) 1888–1908.
[12] L. Codecasa, V. Minerva, M. Politi, Use of barycentric dual grids for the solution of frequency domain problems by FIT, IEEE Trans. Mag. 40 (2) (2004) 1414–1419.
[13] M. Marrone, Properties of constitutive matrices for electrostatic and magnetostatic problems, IEEE Trans. Mag. 40 (3) (2004) 1516–1520.
[14] L. Codecasa, R. Specogna, F. Trevisan, Symmetric positive-definite constitutive matrices for discrete eddy-current problems, IEEE Trans. Mag. 42 (2) (2007) 510–515.
[15] C.R. Anderson, Efficient solution of the SchroedingerPoisson equations in layered semiconductor devices, J. Comput. Phys. 228 (2009) 4745–4756.
[16] T.-M. Hwang, W.-W. Lin, W.-C. Wang, W. Wang, Numerical simulation of three-dimensional pyramid quantum dot, J. Comput. Phys. 196 (2004) 208–232.
[17] H. Voss, Numerical calculation of electronic structure for three-dimensional quantum dot, Comput. Phys. Commun. 174 (2006) 441–446.
[18] S. Lepaul, A. de Lustrac, F. Bouillant, Solving the Poisson's and Schrödinger's equations to calculate the electron states in quantum nanostructures using the finite elemnts method, IEEE Trans. Mag. 32 (3) (1996) 1018–1021.
[19] F. Schwabl, Quantum Mechanics, Springer-Verlag, Berlin, Heidelberg, 1992.
[20] P. Harrison, Quantum Wells, Wires and Dots, Theoretical and Computational Physics, John Wiley & Sons, Chichester, 2000.
[21] T. Tarhasaari, L. Kettunen, A. Bossavit, Some realizations of a discrete Hodge operator: a reinterpretation of finite element techniques, IEEE Trans. Magn. 35 (3) (1999) 1494–1497.
[22] A. Bossavit, Computational Electromagnetism, Academic Press, 1998.
[23] M.E. Gurtin, An Introduction to Continuum Mechanics, Academic Press, 1981.
[24] R. Specogna, F. Trevisan, GAME (Geometric Approach to Maxwell's Equations) code, <http://www.comphys.com>, Copyright 2003–2011.
[25] K. Wu, H. Simon, Thick-restart Lanczos method for large symmetric eigenvalue problems, SIAM J. Matrix Anal. Appl. 22 (2) (2001) 602–616. http://crd.lbl.gov/kewu/trlan.html.